Evolution of nanomorphology and anisotropic conductivity in solvent-modified PEDOT:PSS films for polymeric anodes of polymer solar cells

Seok-In Na,[a] Gunuk Wang,[a] Seok-Soon Kim,[b] Tae-Wook Kim,[a] Seung-Hwan Oh,[c] Byung-Kwan Yu,[a] Takhee Lee[a] and Dong-Yu Kim[*a]

A highly conductive poly(3,4-ethylenedioxythiophene):poly(styrene sulfonate) (PEDOT:PSS) film, obtained by addition of a polar solvent, dimethylsulfoxide (DMSO), to an aqueous solution of PEDOT:PSS, was thoroughly investigated to gain a deeper understanding of the fundamental characteristics of the solvent-modified PEDOT:PSS film. Use of the DMSO-modified PEDOT:PSS film as a transparent anode to achieve low-cost and high-efficiency ITO-free organic solar cells (OSCs) based on poly(3-hexylthiophene) (P3HT) and 1-(3-methoxycarbonyl)-propyl-1-phenyl-(6,6)C_{61} (PCBM) was also examined. Changes in the conductivity, morphology, surface composition, work-function, and anisotropic conductivity in both the parallel and perpendicular directions of solvent-treated PEDOT:PSS films that resulted from the addition of various amounts of DMSO were investigated to better understand the nature of the solvent-modified PEDOT:PSS film and the origin of its dramatically enhanced conductivity. Furthermore, the effects of using the modified PEDOT:PSS films as polymer anodes on solar cell performance were investigated by addition of various amounts of DMSO and by the use of PEDOT:PSS films with different thicknesses. The ITO-free OSCs with optimized PEDOT:PSS anodes had a high power conversion efficiency that was comparable to that of conventional ITO-based devices.

Introduction

The introduction of donor–acceptor heterojunctions made small molecules and conjugated polymers attractive candidates for the fabrication of cost-efficient and flexible power sources.[1,2] In particular, novel organic synthesis and fabrication methods have allowed significant improvements in polymer bulk-heterojunction (BHJ) solar cells that are based on interpenetrating networks of electron-donor and -acceptor materials.[3–13] Despite relatively low efficiency when compared with their inorganic counterparts, potential roll-to-roll processing and large-area processability on low-cost and flexible substrates make conjugated polymer-based organic solar cells (OSCs) very attractive as a cost-effective solution to today's energy-shortage problems.[14,15]

Among the available polymer-based BHJ systems, poly(3-hexylthiophene) (P3HT) and 1-(3-methoxycarbonyl)-propyl-1-phenyl-(6,6)C_{61} (PCBM) networks produced by spin-coating polymer blends have shown the highest efficiency (4–5%) through the optimization of processing parameters such as thermal annealing conditions and solvent evaporation time.[16,17] However, current state-of-the-art OSCs are typically fabricated on rigid glass substrates coated with indium tin oxide (ITO). As a result,

these OSCs do not make full use of the processing advantages of organic materials and limit the realization of fully plastic electronic devices with low cost and high performance, which is an important goal in this field. Furthermore, even among the emergent generation of flexible devices, plastic optoelectronics remain dependent on ITO materials, which have limited mechanical flexibility and readily crack upon substrate bending.[18] In particular, the cost of indium, which is a major component of ITO, prevents large-scale use of ITO in photovoltaic energy conversion. Thus, it is clear that organic-based electrode materials with both high transparency and high conductivity should be developed for low-cost and high-efficiency power generation.

Among the various conducting polymers, poly(3,4-ethylenedioxythiophene) (PEDOT) has attracted considerable interest due to its excellent electrical and optical properties.[19–22] PEDOT is an insoluble polymer, but the use of a water-soluble polyelectrolyte, poly(styrene sulfonic acid) (PSS), as the charge-balancing counterion has made it possible to yield a PEDOT:PSS aqueous composite.[20,21] The PEDOT:PSS composite is one of the most promising organic-based electrode materials owing to its inherent advantages over other conducting polymers such as high transparency in the visible range, long-term stability, and solution processability.[19,20] PEDOT:PSS has been used extensively as an interfacial layer to improve hole-injection in many organic devices. However, the use of PEDOT:PSS as an electrode material has been restricted because commercially available PEDOT:PSS, which is typically used as a buffer layer in organic electronics, has a low conductivity, e.g., $\sim 10^{-3}$ S cm^{-1} (Clevios P VPAI 4083) or $\sim 10^{-5}$ S cm^{-1} (Clevios P CH 8000).[23] Currently, various modified forms of PEDOT:PSS and metal grids to have

[a]Department of Materials Science and Engineering, Department of Nanobio Materials and Electronics, Gwangju Institute of Science and Technology, 1 Oryong-dong, Buk-gu, Gwangju, 500–712, Korea. E-mail: kimdy@gist.ac.kr
[b]Department of Nano and Chemical Engineering, Kunsan National University, Kunsan, Jeollabuk-do, 753–701, Korea
[c]Research Institute for Solar and Sustainable Energies (RISE), 1 Oryong-dong, Buk-gu, Gwangju, 500–712, Korea

even greater conductivities and their potential use as electrodes for ITO-free devices are all being actively investigated.[23–38] For example, despite a limited number of publications,[24–26] a high-conductivity PEDOT:PSS, such as Clevios PH 500, allowed us to fabricate ITO-free OSCs. However, the OSC power conversion efficiencies (∼3%) remained low compared with those of current state-of-the-art OSCs (∼4–5%). Thus, further efforts should be devoted to the achievement of ITO-free OSCs with efficiencies comparable to those of high-performance ITO-based OSCs for low-cost power generation. In addition, although there is significant commercial and scientific interest in the use of highly conductive PEDOT:PSS films as electrodes, key research areas remain to be addressed: the fundamental properties of PEDOT:PSS films that are relevant for application to OSC electrodes; the evolution of electronic and morphological properties with processing; and, the optimal processing parameters for films to be used as anodes in ITO-free cells. More importantly, considering that there is a lack of an in-depth understanding of many aspects of solvent-modified PEDOT:PSS films and that morphology and physical properties such as conductivity can vary dramatically among different PEDOT:PSS formulations that differ in the ratio of conducting PEDOT to insulating PSS or in solid content,[39,40] the correlation between conductive properties and morphology, the origin of the dramatically enhanced conductivity of PEDOT:PSS films following solvent treatment, and the nature of charge transport are still active research areas.

In this study, a highly conductive PEDOT:PSS film, obtained by addition of a polar solvent, dimethylsulfoxide (DMSO), to an aqueous solution of PEDOT:PSS, was investigated to gain a deeper understanding of the fundamental properties of the solvent-modified PEDOT:PSS film. In addition, we examined the use of the solvent-modified PEDOT:PSS film as a transparent anode to achieve low-cost and high-efficiency ITO-free OSCs based on P3HT and PCBM. We investigated a recently developed PEDOT:PSS formulation, Clevios PH 510, which was provided by Starck, as a polymer anode in plastic solar cells. The greater solid content of PH 510, as compared with PH 500, improves its processing for certain applications such as layer-thickness in spin-coating.[23,24] Changes in the conductivity, morphology, surface composition, work-function, and anisotropic conductivity in both the parallel and perpendicular directions of solvent-treated PEDOT:PSS films that resulted from the addition of various amounts of DMSO were investigated to better understand the nature of the solvent-modified PEDOT:PSS film and the origin of its dramatically enhanced conductivity. Furthermore, the effects of using the modified PEDOT:PSS films as polymer anodes on solar cell performance were investigated by the addition of various amounts of DMSO and by the use of PEDOT:PSS films with different thicknesses. The ITO-free OSCs with optimized PEDOT:PSS anodes had a power conversion efficiency that was comparable to that of conventional ITO-based devices.

Experimental

Material characterization

For sample preparation and measurement, glass (Eagle 2000, Corning) substrates were cleaned with a detergent (Mucasol, Merz) followed by ultrasonication in both acetone and isopropyl alcohol and treatment at 100 °C for ∼30 min. Each substrate was treated with UV/ozone to improve the wettability of PEDOT:PSS. PH 510 (Clevios PH 510, provided by H. C. Starck) and DMSO-modified PH 510 solutions were filtered using a 0.45 μm syringe filter. Film conductivity was measured using a standard four-point-probe system with a Keithley 2400 current source and HP 34420A nanovoltmeter. Film thickness was measured using a surface profiler (Kosaka ET-3000i), and the surface images of films were obtained using an atomic force microscope (Park Systems XE-100). XPS measurements were carried out using an AXIS-NOVA (Kratos) system equipped with a monochromatized Al Kα source with a base pressure of 5×10^{-8} Torr, and work function was measured using a Kelvin probe (KP 6500 Digital Kelvin probe, McAllister Technical Services. Co., Ltd.). For the in-plane (∥) electrical measurements, Ti/Au (5 nm/100 nm) electrodes (0.3 × 2 mm, separated by a distance of 8×10^{-2} mm) were evaporated onto the surface of the cleaned substrates. For the out-of-plane (⊥) electrical measurements, the vertical device structures with *via*-hole junctions were fabricated. Ti/Au (5 nm/100 nm) bottom electrodes were evaporated onto the surface of the cleaned substrates. Then, a conventional photolithography process was performed twice to pattern the bottom electrodes and make square *via*-holes with a side length of 90 μm. After the modified PEDOT:PSS films were spin-coated onto the exposed bottom electrode, the top Au (100 nm) electrode was evaporated onto the PEDOT:PSS layer using a shadow mask. The Au top electrode served as a good contact for the probes. The Au electrode was also used as a mask while PEDOT:PSS was etched away using RIE (reactive ion etching) to prevent a direct current path through the PEDOT:PSS film from the top electrode to the bottom electrode. The current–voltage (*I–V*) characteristics of the fabricated devices were carried out using semiconductor parameter analyzers (HP4155A) at room temperature. The UV-Vis transmission spectra were measured using a Perkin-Elmer Lambda 12 UV/Vis spectrophotometer. Cross-sectional TEM images of the ITO-free cell, prepared using a focused ion beam (FIB, NOVA200), were obtained using an FE-TEM (FEI Tecnai F30 S-Twin) operated at 300 kV.
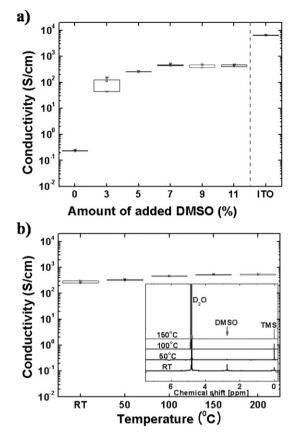
Device fabrication and characterization

For the fabrication of polymer anodes, the modified PH 510 films were spin-coated onto the cleaned glass substrates using a 0.45 μm filter and were subsequently annealed at 150 °C for 30 min. For the fabrication of photoactive layers composed of interconnected networks of electron donors and acceptors, 25 mg of P3HT (4002-E, purchased from Rieke Metals) and 25 mg of PCBM ([60]PCBM, purchased from Nano-C) were dissolved in 1 ml of 1,2-dichlorobenzene. The P3HT and PCBM blend was stirred at 50 °C for ∼12 h in a N_2-filled glove box to obtain a homogeneous mixture. The photoactive layers of each device were formed by spin-coating the mixture, which had been filtered using a 0.2 μm PTFE filter, onto the respective PEDOT:PSS layers. Then, solvent annealing was performed by keeping the spin-coated films inside a covered glass jar for 1 h, followed by thermal annealing at 110 °C for 10 min, forming an active layer with a thickness of ∼230 nm. Device fabrication was completed

by thermal evaporation of a Ca/Al (20 nm/100 nm) metal top electrode with an area of 4.66 mm² under vacuum at a pressure of 10^{-6} Torr. For comparison, conventional ITO-based OSCs were also fabricated using both standard VPAI 4083, which is commonly used as an interfacial layer in ITO-based OSCs, and experimental procedures identical to those used for fabrication of ITO-free OSCs. VPAI 4083 was spin-coated at 5000 rpm for 40 s using a 0.45 μm filter and was subsequently annealed at 150 °C for 30 min, producing a film ~20 nm thick. The photocurrent density–voltage (J–V) curves were measured using a Keithley 4200 source measurement unit. Cell performance was measured under 100 mW cm⁻² illumination intensity generated using a 1 KW Oriel solar simulator with an AM 1.5 G filter in a N₂-filled glove box. For accurate measurement, the light intensity was calibrated using a radiant power meter and a reference silicon solar cell certified by NREL (PVM188 with a KG5 color-filtered window).

Results and discussion

First, we investigated the effects of the amount of added solvent on the electrical properties of the films. Fig. 1a shows the conductivity of PH 510 films that had been modified with various amounts of DMSO; data for both a pure PH 510 film and ITO (Samsung Corning Co., Ltd., ~10 Ω/square) are also presented for comparison. Samples were prepared as follows. PEDOT:PSS was formulated using various amounts of added DMSO. The various preparations were then spin-coated at either 1000, 2000, 3000, or 5000 rpm for 40 s and annealed at 150 °C for 30 min in air. The conductivity of each PEDOT:PSS film was evaluated using four-point-probe measurements. The average conductivity of measurements taken at both the center and edges of each PEDOT:PSS film was then plotted. As shown in Fig. 1a, the conductivity of pure PH 510 (~0.2 S cm⁻¹) was much greater than that of VPAI 4083 (~10⁻³ S cm⁻¹), which is typically used as an interfacial layer for better hole-injection in optoelectronic devices. In particular, conductivity increased with addition of DMSO and then became saturated at a peak conductivity of ~526 S cm⁻¹. The average conductivity of the PH 510 films modified with 7, 9, and 11% DMSO was ~464 S cm⁻¹, which is more than three orders of magnitude greater than that of pure PH 510 and only one order of magnitude less than that of crystalline ITO. In fact, the enhancement of PEDOT:PSS film conductivity by addition of high-boiling solvents and polar compounds is well-known and has been widely studied.[27–33] However, the origin of the enhanced conductivity of PEDOT:PSS films following addition of a polar solvent remains controversial. For example, Kim et al.[27] reported that conductivity can be increased mainly due to the screening effects of polar solvents. Ouyang et al.[28] suggested that conformational changes increase both intra- and inter-chain charge-carrier mobility. Jönsson et al.[31] reported that the excess PSS is washed away from the surface of the PEDOT:PSS grains in the film, leading to a better connection between the conducting PEDOT:PSS grains. Nardes et al.[33] recently reported that sorbitol-induced enhancement of conductivity is due to a reduction in the thickness of the insulating PSS barrier that separates the conducting PEDOT-rich grains. Thus, further efforts are needed to reach a stronger consensus on the origin of the enhanced conductivity.

Fig. 1 Conductivity of PEDOT:PSS films prepared using (a) different amounts of added DMSO or (b) various annealing temperatures. Inset of (b): ¹H-NMR spectra of DMSO-modified PEDOT:PSS films. The PEDOT:PSS films for (a) were prepared by addition of various amounts of DMSO and annealing at 150 °C for 30 min. The PEDOT:PSS films for (b) and the inset of (b) were prepared by addition of 7% DMSO and annealing at their respective temperature for 30 min.

Next, we investigated how thermal treatment affects the dramatic enhancement in film conductivity that results from solvent treatment (Fig. 1a). In addition, we used ¹H-NMR (300 MHz; D₂O; 3-(trimethylsilyl) propionic-2,2,3,3-d₄ acid, sodium salt) to check whether thermal annealing removes DMSO from the PEDOT:PSS films. We fabricated several identical PEDOT:PSS films that varied only in annealing temperature. The films were prepared by addition of 7% DMSO, spin-coating at 1000 rpm for 40 s, followed by annealing for 30 min. The conductivity of each PEDOT:PSS film was evaluated using four-point-probe measurements. A sample of each film was dissolved in D₂O and subjected to ¹H-NMR spectroscopy (JEOL JNM-LA300WB 300 MHz). As shown in Fig. 1b, conductivity increased with annealing temperate and then became saturated. However, we confirmed that the enhancement in conductivity resulting from thermal treatment was less than that induced by addition of the polar solvent (Fig. 1a). More importantly, even though treatment at 100 °C resulted in the disappearance of the DMSO peak from the PEDOT:PSS film, the overall conductivities of the films treated at 100, 150, and 200 °C were similar (as shown in Fig. 1b and its inset). These results suggest that the DMSO itself is not the primary determinant of the enhanced conductivity; rather, a change in PEDOT and PSS that persists

until the DMSO as a processing additive was all evaporated is the key to understanding the dramatic enhancement in the conductivity of the dried PEDOT:PSS films.[29,33]

In general, the secondary and tertiary structure of the PEDOT:PSS complex have been characterized as follows: PEDOT is positively charged due to oxidative polymerization; PEDOT has a low molecular weight (MW); the high MW PSS acts as a template; the negatively charged sulfate groups compensate for PEDOT; PEDOT is linked to PSS by tight ionic bonds; and, PEDOT:PSS forms gel-particles in water.[19,40–42] Aqueous PEDOT:PSS gel-particles merge to form a continuous film, consistent with water evaporation. Finally, a PEDOT:PSS solid film that consists of PEDOT:PSS grains, namely dried gel-particles, with a hydrophobic and highly conductive PEDOT-rich core and a hydrophilic insulating PSS-rich shell are formed.[40] Herein, the morphology of PEDOT:PSS solid films after drying was recorded to investigate possible changes in morphology and the correlation between morphology and conductivity shown in Fig. 1. Fig. 2 and 3 show atomic force microscopy (AFM) topography and phase images of PH 510 films modified by the addition of various amounts of DMSO and use of different annealing temperatures, respectively. Sample preparation for AFM measurements (Fig. 2) was identical to that used for the conductivity measurement shown in Fig. 1a, except that the spin-coating rate was fixed at 1000 rpm for 40 s. In Fig. 3, sample preparation for AFM measurement was identical to that used for the conductivity measurement shown in Fig. 1b. Fig. 2a–d present the topography images of a $1 \times 1\ \mu m^2$ area of the PEDOT:PSS films modified by addition of DMSO. Going from the pure PH 510 (Fig. 2a) to 11% DMSO (Fig. 2d), the size of the PEDOT:PSS particles increased from 50–80 nm to about 110 nm on average, which is consistent with the increase in surface roughness shown in Fig. 3g. In this case, particle size was definitively linked to film conductivity. As the particles became larger, the total number of particle boundaries in a given volume or area decreased. For better comparative studies, phase images of a $1 \times 1\ \mu m^2$ area of the modified PEDOT:PSS films were simultaneously measured, as shown in Fig. 2e–h. PEDOT:PSS grains consist of a PEDOT-rich core and PSS-rich shell,[40] and in the phase images, the hard and soft segments are shown as bright and dark regions, respectively.[32] Thus, it is believed that as the amount of added DMSO increased, the bright PEDOT-rich
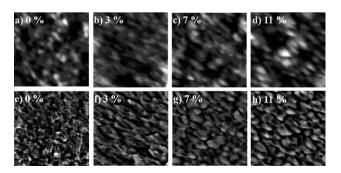

Fig. 3 (a–c) AFM topography and (d–f) phase images of 7% DMSO-modified PH 510 films prepared at various annealing temperatures: (a) and (d), 50 °C; (b) and (e), 100 °C; and, (c) and (f), 200 °C. All images captured an area of $1 \times 1\ \mu m^2$. (g) Surface roughnesses of PH 510 films modified with various amounts of added DMSO and 7% DMSO-modified PH 510 films prepared using various annealing temperatures.

regions in the PEDOT:PSS grains increased in area, while the dark PSS-rich regions became smaller, with a distinct phase separation, indicating that the insulating PSS barrier surrounding or separating highly conductive PEDOT-rich regions was thinner. Compared with the pure PH 510 film shown in Fig. 2a and e, the aforementioned morphological changes were also confirmed by the AFM topography and phase images of modified PH 510 films subjected to different annealing temperatures shown in Fig. 3a–f. The overall morphology of the films treated at 100 and 200 °C was similar to the morphology of films treated at 150 °C, as shown in Fig. 2c and g. These results are consistent with the surface roughness shown in Fig. 3g. More importantly, the observed morphologies shown in Fig. 2 and 3 were highly consistent with the changes in conductivity shown in Fig. 1a and b. From these results, the enhanced conductivity of PH 510 films modified by addition of DMSO can be explained by the morphological changes such as the increase in grain size shown in the topographical images and the thinner PSS barrier shown in the phase images, leading to superior charge-transport pathways among the conducting PEDOT-rich regions.

To complement the aforementioned morphological changes, we used X-ray photoemission spectroscopy (XPS) to investigate the surface chemical composition of modified PH 510 films prepared by the addition of various amounts of DMSO. Sample preparation for XPS measurements was identical to that used for the AFM measurements shown in Fig. 2, and XPS measurements were performed using grazing emission to increase the surface sensitivity.[32] Fig. 4 presents S (sulfur) 2p spectra of the

Fig. 2 AFM topography (a–d) and phase images (e–h) of PH 510 films modified with various amounts of added DMSO: (a) and (e), 0%; (b) and (f), 3%; (c) and (g), 7%; and, (d) and (h), 11%. All images captured an area of $1 \times 1\ \mu m^2$.
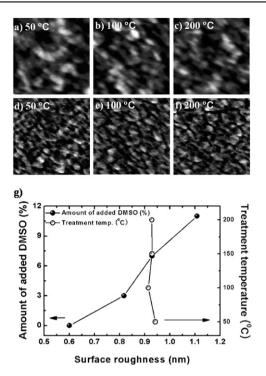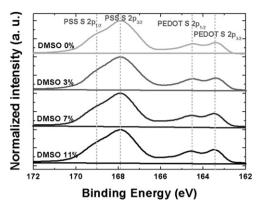
Fig. 4 S 2p spectra of PEDOT:PSS films modified with various amounts of DMSO.

Fig. 5 Work function of PEDOT:PSS films modified with various amounts of DMSO.

PEDOT:PSS films modified with DMSO. The higher binding energy peaks at 169 and 167.8 eV and the lower binding energy peaks at 164.6 and 163.4 eV correspond to the sulfur atoms in PSS and PEDOT, respectively. The ratios of PSS to PEDOT were calculated using the ratio of the areas of the S $2p_{1/2}$ and $2p_{3/2}$ peaks in PSS and PEDOT listed in Table 1. The calculated ratio of PSS to PEDOT reflects the surface composition within ~4 nm because the probing depth is given by $3\lambda\sin\theta$, where the inelastic mean free path (λ) of a S 2p electron is 2.7 nm and the take-off angle (θ) is 30°.[43] As shown in Table 1, it can be confirmed that in the modified PEDOT:PSS films, the PSS-to-PEDOT ratios at the surface were decreased by the addition of DMSO. The variations in the PSS-to-PEDOT ratio at the surface will result in a change in work function, because the reduced concentration of PSS at the film surface can lead to an increase in the density of filled states close to the Fermi level.[43,44] Fig. 5 presents work functions for the PEDOT:PSS films modified by addition of DMSO. Sample preparation was identical to that used for the XPS measurements, and the work function was measured using a Kelvin probe. In fact, as shown in Fig. 5, the work function tended to decrease as the amount of added DMSO increased, thus supporting that the PSS-to-PEDOT ratio was reduced at the film surface, as shown in Table 1. These changes in XPS and work function shown in Fig. 4 and 5 were consistent with the morphological changes, such as enlarged PEDOT-rich regions and thinner PSS barriers, as shown in Fig. 2. More importantly, considering that the XPS S 2p spectra of PEDOT:PSS films gave a surface sulfonate-to-thiophene ratio equivalent to the surface PSS-to-PEDOT ratio,[32] and the bulk PSS-to-PEDOT ratio was equivalent to the ratio of PSS to PEDOT (2.5 : 1) in the PH 510 solution,[39,40] the XPS data indicate that the surface of pure PH 510 film was enriched in PSS and that a composition gradient

Table 1 Ratios of PSS to PEDOT (PSS/PEDOT) at the surface of PEDOT:PSS films modified with various amounts of DMSO
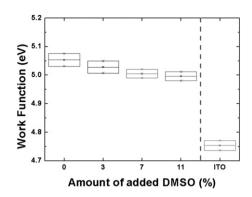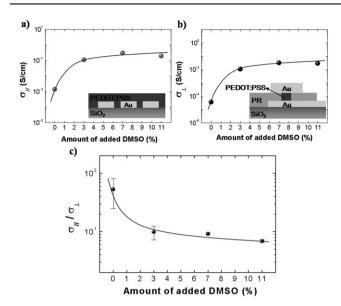
Amount of added DMSO (%)	PSS/PEDOT at surface
0	3.746
3	3.405
7	3.345
11	3.251

existed between the surface and the bulk.[45,46] Nevertheless, the surface PSS-to-PEDOT ratios of the modified PH 510 films approached the bulk PSS-to-PEDOT ratio as the amount of added DMSO increased. Therefore, it is likely that in DMSO-modified PH 510 films, PEDOT molecules that are responsible for conduction in the blend are more uniformly distributed through the entire PEDOT:PSS film and that the morphological changes shown in Fig. 2, such as enlarged PEDOT-rich regions and thinner PSS barriers, occurred throughout the entire PEDOT:PSS film, suggesting that conductivity was uniform over the film and did not vary in either the parallel or perpendicular direction.

To strengthen the aforementioned interpretation, we investigated changes in anisotropic conductivity of modified PEDOT:PSS films in both the parallel and perpendicular directions. Recently, Nardes *et al.*[47,48] showed that, in spin-coated PEDOT:PSS films (VPAI 4083), the dc conductivities measured in the lateral and vertical directions are highly anisotropic. The lateral conductivity was as high as three orders of magnitude greater than the vertical conductivity and was highly correlated with the morphology observed using both scanning tunneling microscopy and cross-sectional AFM.[47,48] Investigation of anisotropic conductivity is likely the most direct way to experimentally study changes in morphology and charge transport that occur throughout the entire PEDOT:PSS film. Devices with different electrode configurations were designed for the in-plane (∥) and out-of-plane (⊥) electrical measurements, as shown in the insets of Fig. 6a and b. Sample preparation for each PEDOT:PSS film was identical to that used for the AFM and XPS measurements shown in Fig. 2 and 4. As shown in Fig. 6a and b, it can be confirmed that as the amount of added DMSO increased, the parallel (∥) and perpendicular (⊥) conductivities of the modified PEDOT:PSS films increased and tended to become saturated. These results suggest decreased spacing and improved connectivity between the PEDOT-rich regions in both the perpendicular and parallel directions. The ratio of parallel (∥) conductivity to perpendicular (⊥) conductivity ($\sigma_\parallel/\sigma_\perp$) is presented in Fig. 6c. Fig. 6c clearly shows that as the amount of added DMSO increased, the anisotropic nature of charge transport in the pure PH 510 film decreased, and the charge transport tended to approach the isotropic charge transport. This finding suggests that in DMSO-modified PH 510 films, PEDOT-rich regions were more uniformly distributed

This journal is © The Royal Society of Chemistry 2009

J. Mater. Chem., 2009, **19**, 9045–9053 | 9049

Fig. 6 Changes in parallel ($\sigma_{\parallel}$) and perpendicular ($\sigma_{\perp}$) conductivities of PEDOT:PSS films modified by addition of various amounts of DMSO: (a) parallel conductivity ($\sigma_{\parallel}$) in modified PEDOT:PSS films; (b) perpendicular conductivity ($\sigma_{\perp}$) in modified PEDOT:PSS films; and, (c) ratios of parallel ($\parallel$) conductivity to perpendicular ($\perp$) conductivity ($\sigma_{\parallel}/\sigma_{\perp}$) in modified PEDOT:PSS films. Insets of (a) and (b): structures of the devices designed for the in-plane ($\parallel$) and out-of-plane ($\perp$) electrical measurements.

throughout the entire PEDOT:PSS film. Moreover, the morphological changes, such as enlarged PEDOT-rich regions and thinner PSS barriers, occur in all parallel and perpendicular directions. Based on these results, the enhancement of conductivity in DMSO-modified PEDOT:PSS films is believed to arise from both the morphological changes that take place in all parallel and perpendicular directions and the more uniform distributions of PEDOT-rich regions throughout the PEDOT:PSS films, leading to superior charge-transport pathways and better connections between PEDOT-rich regions in both the parallel and perpendicular directions.
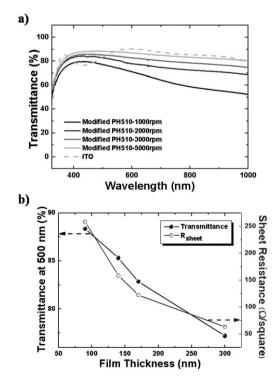
We turn our attention now to the application of the modified PH 510 film as a transparent anode in ITO-free organic solar cells. Fig. 7 shows both the structure of a solar cell with a PEDOT:PSS anode and a high-resolution transmission electron microscopy (TEM) cross-sectional image of a representative ITO-free organic solar cell (IFOSC). The highly conductive polymer anode first layer was prepared by addition of 7% DMSO to PH 510. Although use of DMSO at concentrations greater than 7% also produced high conductivities, it was difficult to

cover the entire glass substrate with a homogeneous layer, which is another important factor affecting cell efficiency and cell characterization. With regard to both conductivity and film uniformity, addition of 7% DMSO was considered the optimal condition for cell fabrication. The second layer, a bulk-heterojunction film composed of interconnected networks of electron-donor and -acceptor materials, was prepared by spin-coating a mixture of P3HT and PCBM. Finally, the calcium and aluminium in the third layer were thermally evaporated to form the cathode.

Because materials that are used as anodes in photovoltaic cells require both high transparency and high conductivity, optical transmission spectra of modified PH 510 films on glass substrates were measured (Fig. 8a); the transmittance of ITO on a glass substrate was also measured for comparison. The modified PH 510 films were prepared by addition of 7% DMSO and spin-coating at either 1000, 2000, 3000, or 5000 rpm for 40 s, followed by annealing at 150 °C for 30 min. As shown in Fig. 8a, it can be confirmed that compared with ITO, most of the modified PH 510 films showed relatively good transparency in the full visible range, in particular in the wavelength range of 400–600 nm, which is the main absorption region of photoactive P3HT. Fig. 8b shows both transmittance and sheet resistance as a function of the thickness of the modified PEDOT:PSS films. The transmittance of each PEDOT:PSS film at a wavelength of 500 nm was plotted. Sheet resistance, which is another important property of transparent and conductive electrodes, was measured using the four-point-probe method. The transmittance and sheet resistance ranged from 77.2 to 88.3% and from 63 to 258 Ω/square, respectively, and were dependent on film thickness.

Fig. 7 Device structure and TEM cross-sectional image (scale bar: 100 nm) of the polymer solar cell with a PEDOT:PSS anode.
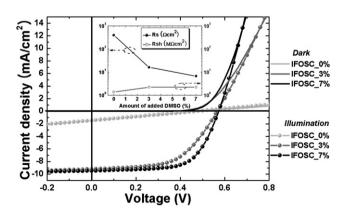
Fig. 8 (a) Optical transmission spectra of modified PH 510 films on glass substrates. (b) Transmittance and sheet resistance as a function of the thickness of the modified PEDOT:PSS films.

More importantly, electrodes used as plastic components in flat panel displays require a sheet resistance of 200–400 Ω/square and a transmittance greater than 80%.[49] Thus, it is believed that the properties of the modified PH 510 films shown in Fig. 8 are sufficient for use as transparent electrodes in organic-based devices.

To directly investigate the potential use of modified PH 510 films as anodes for IFOSCs and the effects of conductivity on IFOSC performance, solar cells with different PEDOT:PSS films spin-coated at 3000 rpm were fabricated and compared. Fig. 9 shows photocurrent density–voltage (J–V) curves measured under 100 mW cm^{-2} illumination with AM 1.5 G conditions. The series resistance (R_s) and shunt resistance (R_{sh}) obtained from the dark curves of solar cells are shown in the inset of Fig. 9. Devices with PH 510 films modified by addition of either 3 or 7% DMSO exhibited excellent performance characteristics, respectively: short circuit current (J_{sc}), 9.204 and 9.471 mA cm^{-2}; open circuit voltage (V_{oc}), 0.564 and 0.572 V; fill-factor (FF), 55.9 and 64.2%; and, power conversion efficiency (η_p), 2.90 and 3.48%. By contrast, the pure PH 510 film exhibited very poor performance characteristics and did not function as an electrode. The dramatic enhancement in cell performance that results from addition of DMSO was attributed to the significant increase in the conductivity of the modified PEDOT:PSS films (Fig. 1a), which was confirmed by the much higher FF (Fig. 9) and much lower R_s (Fig. 9 inset) of the solar cells made with DMSO-modified films.
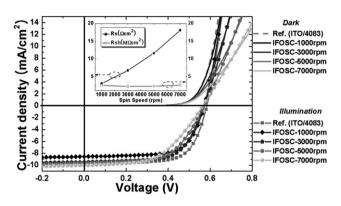
To investigate the effect of the thickness of DMSO-modified PH 510 anodes on IFOSC performance, we fabricated several OSCs that varied only in their respective anodes. The modified PH 510 anodes were prepared by addition of 7% DMSO and spin-coating at either 1000, 3000, 5000, or 7000 rpm for 40 s. ITO/VPAI 4083 was also prepared for use as a reference anode in conventional OSCs. The J–V characteristics of the cells under illumination and in the dark are shown in Fig. 10. Detailed information regarding η_p, J_{sc}, V_{oc}, and FF, which were calculated from the J–V curves in Fig. 10, is presented in Table 2. As shown in Fig. 10 and Table 2, FF values in cells with modified PH 510 anodes increased with film thickness. In general, the FF was tightly linked to both R_s and R_{sh}. The increase in FF for the IFOSCs with increasing anode thickness can be attributed to

Table 2 Photovoltaic parameters and efficiency of ITO-free OSCs with DMSO-modified PH 510 anodes and a reference ITO-based OSC

	η_p (%)	J_{sc}/mA cm^{-2}	V_{oc}/V	FF (%)
Ref. (ITO/4083)	3.89	9.792	0.584	68.0
IFOSC-1000 rpm	3.29	8.530	0.571	67.5
IFOSC-3000 rpm	3.48	9.471	0.572	64.2
IFOSC-5000 rpm	3.27	9.640	0.572	59.3
IFOSC-7000 rpm	2.99	10.03	0.564	52.9

Fig. 10 J–V characteristics of ITO-free solar cells with modified PH 510 anodes and a conventional solar cell with an ITO/VPAI 4083 reference anode. Inset: R_s and R_{sh} obtained from the dark curves of solar cells with DMSO-modified PH 510 anodes prepared using different spin-coating rates.

either a decrease in R_s, an increase in R_{sh}, or both. We then calculated R_s and R_{sh} from the dark curves of solar cells with modified PH 510 anodes, and each parameter was plotted in the inset of Fig. 10. The R_s values in cells with modified PH 510 anodes decreased with increasing anode thickness, while values of R_{sh} were relatively constant, irrespective of the film thickness. Furthermore, R_s is the sum of the contact resistance and the bulk resistance of the materials, and all materials and processes used to fabricate the cells were identical, except for the thickness of the modified PH 510 anodes. Therefore, the R_s and FF of the cells were dependent only on the sheet resistance of the modified PH 510 anode shown in Fig. 8b. Although, in the IFOSC-1000 rpm cell, FF increased due to a decrease in R_{sheet} as film thickness increased, J_{sc} was reduced. This result was attributed to the decrease in transmittance as film thickness increased (Fig. 8). As a result, the ITO-free solar cell with the modified PH 510 anode that was spin-coated at 3000 rpm showed the highest efficiency. It is worth noting that the photovoltaic characteristics of the IFOSC-3000 rpm cell were comparable to those of conventional OSCs with crystalline-ITO, as shown in Fig. 10 and Table 2. In addition, all ITO-free OSC characteristics clearly demonstrate that the highly conductive polymer material shows potential as a practical replacement for expensive crystalline-ITO on glass or brittle amorphous-ITO on a flexible substrate.

Conclusions

Highly conductive PEDOT:PSS films, obtained by addition of a polar solvent (DMSO) to a recently developed aqueous solution of PEDOT:PSS (PH 510), were investigated. Changes in the

Fig. 9 J–V characteristics of solar cells with DMSO-modified PH 510 anodes prepared by addition of various amounts of DMSO. Inset: R_s and R_{sh} obtained from the dark curves of solar cells with modified PH 510 anodes prepared by addition of various amounts of DMSO.

This journal is © The Royal Society of Chemistry 2009

J. Mater. Chem., 2009, **19**, 9045–9053 | 9051

conductivity, morphology, surface composition, work-function, and anisotropic conductivities in both the parallel and perpendicular directions of solvent-modified PEDOT:PSS films that resulted from addition of various amounts of DMSO were investigated to understand both the nature of the modified PEDOT:PSS film and the origin of its dramatically enhanced conductivity. AFM phase images of the DMSO-modified PH 510 films showed morphological changes such as an enlarged PEDOT-rich region and a thinner PSS barrier. Investigation of anisotropic conductivity of solvent-modified PEDOT:PSS films in both the parallel and perpendicular directions showed that as the amount of added DMSO increased, the charge transport in the pure PH 510 film became less anisotropic and more isotropic in nature. This finding suggests that in DMSO-modified PH 510 films, PEDOT-rich regions were more uniformly distributed throughout the entire PEDOT:PSS film. Moreover, the morphological changes, such as enlarged PEDOT-rich regions and thinner PSS barriers, occur in all parallel and perpendicular directions. Based on the observed changes in morphology, surface composition, and anisotropic conductivity, the enhancement of conductivity in DMSO-modified PEDOT:PSS films is believed to arise from both the morphological changes and the more uniform distributions of PEDOT-rich regions throughout the PEDOT:PSS films, leading to superior charge-transport pathways and better connections between PEDOT-rich regions in both the parallel and perpendicular directions. Furthermore, the effects of using the modified PEDOT:PSS films as polymer anodes on solar cell performance were investigated by addition of various amounts of DMSO and by use of PEDOT:PSS films with different thicknesses. The overall photovoltaic characteristics of the ITO-free OSC with an optimized PEDOT:PSS anode were comparable to those of conventional ITO-based devices, demonstrating that the highly conductive polymeric material shows potential as a practical replacement for expensive crystalline-ITO on glass or brittle amorphous-ITO on flexible substrates. The results of the present study will allow full use of the highly conductive PEDOT:PSS films and will advance the production of low-cost and high-efficiency OSCs by high-throughput roll-to-roll manufacturing.

References

1 C. W. Tang, *Appl. Phys. Lett.*, 1986, **48**, 183.
2 N. S. Sariciftci, L. Smilowitz, A. J. Heeger and F. Wedl, *Science*, 1992, **258**, 1474.
3 C. J. Brabec, N. S. Sariciftci and J. C. Hummelen, *Adv. Funct. Mater.*, 2001, **11**, 15.
4 X. Yang, J. Loos, S. C. Veenstra, W. J. H. Verhees, M. M. Wienk, J. M. Kroon, M. A. J. Michels and R. A. J. Janssen, *Nano Lett.*, 2005, **5**, 579.
5 Y. Kim, S. Cook, S. M. Tuladhar, S. A. Choulis, J. Nelson, J. R. Durrant, D. D. C. Bradley, M. Giles, I. Mcculloch, C.-S. Ha and M. Ree, *Nat. Mater.*, 2006, **5**, 197.
6 F. C. Krebs and H. Spanggaard, *Chem. Mater.*, 2005, **17**, 5235.
7 S.-S. Kim, S.-I. Na, J. Jo, G. Tae and D.-Y. Kim, *Adv. Mater.*, 2007, **19**, 4410.
8 X. Yang, G. Lu, L. Li and E. Zhou, *Small*, 2007, **3**, 611.
9 F. C. Krebs, *Sol. Energy Mater. Sol. Cells*, 2009, **93**, 394.
10 J. Y. Kim, K. Lee, N. E. Coates, D. Moses, T.-Q. Nguyen, M. Dante and A. J. Heeger, *Science*, 2007, **317**, 222.
11 J. Peet, J. Y. Kim, N. E. Coates, W. L. Ma, D. Moses, A. J. Heeger and G. C. Bazan, *Nat. Mater.*, 2007, **6**, 497.
12 S.-I. Na, S.-S. Kim, J. Jo, S.-H. Oh, J. Kim and D.-Y. Kim, *Adv. Funct. Mater.*, 2008, **18**, 3956.
13 M.-G. Kang, M.-S. Kim, J. Kim and L. J. Guo, *Adv. Mater.*, 2008, **20**, 4408.
14 F. C. Krebs, S. A. Gevorgyan and J. Alstrup, *J. Mater. Chem.*, 2009, **19**, 5442.
15 F. C. Krebs, *Org. Electron.*, 2009, **10**, 761.
16 W. Ma, C. Yang, X. Gong, K. Lee and A. J. Heeger, *Adv. Funct. Mater.*, 2005, **15**, 1617.
17 G. Li, V. Shrotriya, J. Huang, Y. Yao, T. Moriarty, K. Emery and Y. Yang, *Nat. Mater.*, 2005, **4**, 864.
18 Z. Chen, B. Cotterell, W. Wang, E. Guenther and S.-J. Chua, *Thin Solid Films*, 2001, **394**, 201.
19 S. Kirchmeyer and K. Reuter, *J. Mater. Chem.*, 2005, **15**, 2077.
20 L. Groenendaal, F. Jonas, D. Freitag, H. Pielartzik and J. R. Reynolds, *Adv. Mater.*, 2000, **12**, 481.
21 B. Winther-Jensen and K. West, *Macromolecules*, 2004, **37**, 4538.
22 B. Winther-Jensen and F. C. Krebs, *Sol. Energy Mater. Sol. Cells*, 2006, **90**, 123.
23 H. C. Starck homepage. http//:www.baytron.com (last accessed March 2009).
24 S.-I. Na, S.-S. Kim, J. Jo and D.-Y. Kim, *Adv. Mater.*, 2008, **20**, 4061.
25 Y. Zhou, F. Zhang, K. Tvingstedt, S. Barrau, F. Li, W. Tian and O. Inganäs, *Appl. Phys. Lett.*, 2008, **92**, 233308.
26 E. Ahlswede, W. Mühleisen, M. W. bin Moh Wahi, J. Hanisch and M. Powalla, *Appl. Phys. Lett.*, 2008, **92**, 143307.
27 J. Y. Kim, J. H. Jung, D. E. Lee and J. Joo, *Synth. Met.*, 2002, **126**, 311.
28 J. Ouyang, C.-W. Chu, F.-C. Chen, Q. Xu and Y. Yang, *Adv. Funct. Mater.*, 2005, **15**, 203.
29 J. Huang, P. F. Miller, J. S. Wilson, A. J. de Mello, J. C. de Mello and D. D. C. Bradley, *Adv. Funct. Mater.*, 2005, **15**, 290.
30 L. A. A. Pettersson, S. Ghosh and O. Inganäs, *Org. Electron.*, 2002, **3**, 143.
31 S. K. M. Jönsson, J. Birgerson, X. Crispin, G. Greczynski, W. Osikowicz, A. W. Denier van der Gon, W. R. Salaneck and M. Fahlman, *Synth. Met.*, 2003, **139**, 1.
32 X. Crispin, F. L. E. Jakobsson, A. Crispin, P. C. M. Grim, P. Andersson, A. Volodin, C. van Haesendonck, M. Van der Auweraer, W. R. Salaneck and M. Berggren, *Chem. Mater.*, 2006, **18**, 4354.
33 A. M. Nardes, R. A. J. Janssen and M. Kemerink, *Adv. Funct. Mater.*, 2008, **18**, 865.
34 T. Aernouts, P. Vanlaeke, W. Geens, J. Poortmans, P. Heremans, S. Borghs, R. Mertens, R. Andriessen and L. Leenders, *Thin Solid Films*, 2004, **451–452**, 22.
35 J.-Y. Lee, S. T. Connor, Y. Cui and P. Peumans, *Nano Lett.*, 2008, **8**, 689.
36 M. Strange, D. Plackett, M. Kaasgaard and F. C. Krebs, *Sol. Energy Mater. Sol. Cells*, 2008, **92**, 805.
37 K. Tvingstedt and O. Inganäs, *Adv. Mater.*, 2007, **19**, 2893.
38 B. Zimmermann, M. Glatthaar, M. Niggemann, M. K. Riede, A. Hinsch and A. Gombert, *Sol. Energy Mater. Sol. Cells*, 2007, **91**, 374.

9052 | *J. Mater. Chem.*, 2009, **19**, 9045–9053

This journal is © The Royal Society of Chemistry 2009

39 A. Elschner and S. Kirchmeyer, in *Organic Photovoltaics: Materials, Device Physics, and Manufacturing Technologies*, ed. C. J. Brabec, V. Dyakonov and U. Scherf, Wiley-VCH, Weinheim, 2008.
40 U. Lang, E. Müller, N. Naujoks and J. Dual, *Adv. Funct. Mater.*, 2009, **19**, 1215.
41 S. Ghosh and O. Inganäs, *Synth. Met.*, 1999, **101**, 413.
42 F. Jonas and G. Heywang, *Electrochim. Acta*, 1994, **39**, 1345.
43 T.-W. Lee and Y. Chung, *Adv. Funct. Mater.*, 2008, **18**, 2246.
44 G. Greczynski, Th. Kugler, M. Keil, W. Osikowicz, M. Fahlman and W. R. Salaneck, *J. Electron Spectrosc. Relat. Phenom.*, 2001, **121**, 1.
45 P. C. Jukes, S. J. Martin, A. M. Higgins, M. Geoghegan, R. A. L. Jones, S. Langridge, A. Wehrum and S. Kirchmeiyer, *Adv. Mater.*, 2004, **16**, 807.
46 G. Greczynski, Th. Kugler and W. R. Salaneck, *Thin Solid Films*, 1999, **354**, 129.
47 A. M. Nardes, M. Kemerink, R. A. J. Janssen, J. A. M. Bastiaansen, N. M. M. Kiggen, B. M. W. Langeveld, A. J. J. M. Van Breemen and M. M. de Kok, *Adv. Mater.*, 2007, **19**, 1196.
48 A. M. Nardes, M. Kemerink and R. A. J. Janssen, *Phys. Rev. B: Condens. Matter Mater. Phys.*, 2007, **76**, 085208.
49 J.-Y. Kim, M.-H. Kwon, Y.-K. Min, S. Kwon and D.-W. Ihm, *Adv. Mater.*, 2007, **19**, 3501.

This journal is © The Royal Society of Chemistry 2009

J. Mater. Chem., 2009, **19**, 9045–9053 | 9053